Murilo Tomazini Munhoz Moya, Leandro Goulart de Araujo*, Fernando Silva Lopes and Antonio Carlos Silva Costa Teixeira*

TiO_2 P25 and Kronos vlp 7000 materials activated by simulated solar light for atrazine degradation

https://doi.org/10.1515/ijcre-2022-0186
Received September 23, 2022; accepted May 29, 2023;
published online June 12, 2023

Abstract: Photocatalysis-based technologies have been proposed for the treatment of wastewater containing atrazine (ATZ), a persistent and recalcitrant pollutant. This study aims to evaluate and compare the efficiency of TiO_2 P25 and TiO_2 modified with carbon (C–TiO_2 Kronos vlp 7000) in the photocatalytic degradation of ATZ in aqueous systems. The experiments were performed in a tubular photochemical reactor equipped with a compound parabolic collector (CPC) irradiated by simulated solar light. The materials were characterized by X-ray diffraction, infrared spectroscopy, BET specific surface area, and diffuse reflectance spectroscopy. For TiO_2 P25, ATZ removals varied in the range 86–100 % after 120 min of irradiation, although the total organic carbon (TOC) analyses indicated that no significant ATZ mineralization occurred (<20 %). C–TiO_2 Kronos vlp 7000, on the other hand, was not able to completely remove ATZ after 120 min of irradiation. In this case, pesticide removals were 37–45 % over 120 min, while C–TiO_2 performed better with regard to ATZ mineralization, with 38 % TOC removal. Given the low mineralization of atrazine, the intermediate compounds formed were identified for each photocatalytic material.

Present address: Institut Jean Lamour, CNRS UMR7198, Université de Lorraine, Ecole Nationale Supérieure des Technologies et Industries du Bois (ENSTIB), 27 Rue Philippe Séguin, BP 1041, 88051 Epical Cedex 9, France.

***Corresponding authors: Leandro Goulart de Araujo**, Instituto de Pesquisas Energéticas e Nucleares, IPEN/CNEN, Av. Prof. Lineu Prestes, 2242, 05508-000, São Paulo, SP, Brazil, E-mail: lgoulart@alumni.usp.br. https://orcid.org/0000-0002-9358-0942; and **Antonio Carlos Silva Costa Teixeira**, Research Group in Advanced Oxidation Processes (AdOx), Department of Chemical Engineering, Escola Politécnica, University of São Paulo (USP), Av. Prof. Luciano Gualberto, Travessa 3, 380, 05508-010, São Paulo, SP, Brazil, E-mail: acscteix@usp.br

Murilo Tomazini Munhoz Moya, Research Group in Advanced Oxidation Processes (AdOx), Department of Chemical Engineering, Escola Politécnica, University of São Paulo (USP), Av. Prof. Luciano Gualberto, Travessa 3, 380, 05508-010, São Paulo, SP, Brazil

Fernando Silva Lopes, Instituto de Química, University of São Paulo (USP), Av. Prof. Lineu Prestes, 748, 05508-000, São Paulo, SP, Brazil

Keywords: by products; carbon-doped titanium dioxide; herbicide; kinetics; photocatalysis

1 Introduction

Atrazine (ATZ) is an herbicide that presents a significant risk to the aquatic environment and has been included in the list of priority pollutants in the European Union (No 2001). After establishing a maximum of 0.1 μg L^{-1} ATZ concentration in drinking water and groundwater, the European Union decided to ban ATZ in light of new evidence of its toxicity (de Albuquerque et al. 2020). In Germany, for example, its use has been prohibited since 1991. Nevertheless, a much higher concentration of ATZ and its chloro-s-triazine metabolites in drinking water (100 μg L^{-1}) is allowed by the World Health Organization (WHO 2003). Other examples of maximum ATZ concentrations permissible are those from the United States (3 μg L^{-1}) (EPA 2009) and Brazil (2 μg L^{-1}) for freshwater (Conama 2005). Nevertheless, in the USA, Brazil, and Argentina, ATZ is one of the most widely used herbicides in grain cultivations. As a consequence, the herbicide is repeatedly detected in ground and surface water in these regions (Bonansea, Amé, and Wunderlin 2013). According to Wu et al. (2018), the rationale is that ATZ presents moderate aqueous solubility (33 mg L^{-1}, 27 °C), relatively long half-life (30–100 days), and high mobility. The main issue is that it is commonly detected in concentration values above those established in regulations, such as those from the EU (Wu et al. 2018). Examples of measured concentrations found worldwide are 0.01–6 μg L^{-1} in groundwater and 0.01–5 μg L^{-1} in drinking-water (WHO 2003). Other widespread issues are related to the presence of ATZ in soil because its metabolites/residues frequently persist in agricultural fields and water bodies for years (Singh et al. 2020).

In recent years, many literature records have demonstrated that advanced oxidation processes (AOPs) are especially useful for degrading persistent contaminants such as dyes (Serrano-Martínez et al. 2020), antibiotics (Mukimin, Vistanty, and Zen 2020), industrial chemicals (de Araujo et al. 2020a), and ATZ (Komtchou et al. 2020). The paramount advantages of using AOPs are (1) fast degradation rate, (2) possibility of partial or total mineralization of organic

compounds into CO_2, H_2O and other inorganic products, (3) suitability to operate under ambient pressure and temperature, and (4) potential to reduce the toxicity of organic contaminants (Ong, Ng, and Mohammad 2018). The efficiency of these techniques is given by the high rates of oxidation by hydroxyl radicals, which can degrade a wide range of organic molecules. These radicals hold low selectivity (de Araujo et al. 2020b), with second-order rate constants in the range 10^{10}–10^{12} L mol^{-1} s^{-1}.

Among the AOPs, photocatalysis stands out as a promising technique for degrading persistent organic pollutants owing to low energy consumption, no extra pollution, and controlled reaction conditions (Wang et al. 2020). The selection of the proper photocatalyst in this scenario is crucial. The benefits of suspending photocatalysts in aqueous solutions are (i) low-pressure drop within the reactor, (ii) the excellent mass transfer of contaminants present in the liquid phase onto active surface sites of photocatalysts, and (iii) easiness of adsorption and desorption of the pollutants over the reaction (Ong, Ng, and Mohammad 2018). Despite the drawback of the catalyst recovery cost, heterogeneous photocatalysis exhibits the perks of a broad spectrum of organic compounds that can be mineralized, additional electron acceptors are often unneeded, and possible photocatalyst re-usage (Cai et al. 2020; Suri et al. 1993). Furthermore, the use of solar radiation as the light source to activate the catalyst is considered a more cost-effective alternative (Ong, Ng, and Mohammad 2018).

Among the variety of semiconductors, TiO_2 is the most used in photocatalytic processes for comprising acceptable band gap, chemical endurance, high proficiency to adsorb electrons and it is affordable (Gani and Kazmi 2016). According to Lee, Palaniandy, and Dahlan (2017), the commercial crystalline TiO_2 powder (Evonik P25) in its two typically configurations (25:75 or 80:20 anatase:rutile) is the most utilized heterogeneous catalyst in treatment processes. The reason is its chemical stability, low toxicity and availability for oxidation processes (Al-Rasheed 2005; Spasiano et al. 2015). In addition, different investigations are reported in the literature, in which modified TiO_2 has been applied to degrade ATZ in aqueous matrices. For example, Cheshme Khavar et al. (2020) proposed a new Ru(II) polypyridyl complex for enhancing the visible-light-driven photocatalytic activity of a TiO_2/reduced graphene oxide nanocomposite. The catalysts presented a rate of ATZ degradation nine times higher than that exhibited by the commercial TiO_2 P25, which was attributed to the better light harvesting and efficient electron transportation of the material. Cruz et al. (2017) studied the degradation of a mixture of pesticides by bare TiO_2 and graphene oxide photocatalysts (GO-TiO_2) under simulated sunlight, confirming that the later presented higher photocatalytic activity, higher degradation rates and faster chloride formation. Romão and Mul (2016) compared three photocatalysts (TiO_2 P25, TiO_2 Hombikat and Pt (0.5 %)-promoted P25 at concentrations 0.25–2 g L^{-1}) in the degradation of the mixture of methyl orange and ATZ in aqueous solutions. TiO_2 P25 performed better in the decomposition of methyl orange and ATZ at 0.25 g L^{-1} when compared to Hombikat and Pt/P25. Yang et al. (2015) compared the efficiency of anatase TiO_2 films with that of commercial P25 TiO_2 using $[ATZ]_0$ = 10 mg L^{-1} and UV light; the as-synthesized films demonstrated greater performance for degrading ATZ and acid orange II.

In comparison with several studies on the use of TiO_2 P25 in the photocatalytic degradation of pollutants, the use of the carbon-modified material C–TiO_2 Kronos vlp 7000 has been scarcely evaluated. Manassero, Satuf, and Alfano (2013) studied the photocatalytic activity under UV, visible, and UV-visible radiation of P25 and Kronos vlp 7000 for water remediation in a slurry reactor. The later showed absorption in the visible range and was about three-fold more efficient than P25 in bisphenol A degradation. Conversely, under UV radiation, the quantum efficiency of P25 was 1.5-fold higher than that of Kronos vlp 7000. Fotiou et al. (2016) investigated the photocatalytic removal of cyanotoxins (MC-LR and CYN), water taste and odor. For that, the authors employed TiO_2 P25 and Kronos vlp 7000 TiO_2 with an eye toward the roles of reactive oxygen species under UV and visible light, showing that both cyanotoxins could be removed under visible-radiation, but not water taste and odor. Vela et al. (2018) investigated the photocatalytic oxidation of six pesticides (malathion, fenitrothion, quinalphos, vinclozoline, dimethoate, and fenarimol) in wastewater by TiO_2 P25 and Kronos vlp 7000 under sunlight irradiation, at the initial concentration of 0.3 mg L^{-1} each. In all experimental conditions evaluated, TiO_2 P25 was found to be two-fold more efficient than TiO_2 vlp 7000. Berberidou et al. (2019) employed varieties of TiO_2-based materials (TiO_2 UV-100, TiO_2 Kronos uvlp 7500, TiO_2 P25, and TiO_2 Kronos vlp 7000) for studying the decomposition and detoxification of the insecticide thiacloprid. TiO_2 P25 depicted the highest efficiency among the tested commercial TiO_2, while C-doped TiO_2 Kronos vlp 7000 was unable to degrade thiacloprid under UV-A and visible light. Kitsiou et al. (2018) studied the mineralization of the drug carboplatin with TiO_2 P25 under UV-A, and C-doped TiO_2 Kronos vlp 7000 under UV-A and visible light, with TiO_2 P25 showing the best results. Spyrou et al. (2022) investigated the use of C-doped TiO_2 Kronos vlp 7000 under UV-A and

visible irradiation for the photocatalytic degradation of cimetidine and amisulpride. After 35 min of exposure to UV-A, cimetidine degradation reached 85.7 %, while under visible radiation, the degradation percentage was 64.4 % after 120 min. Likewise, amisulpride degradation was 86.6 % after 120 min of UV-A exposure and 58.1 % under visible irradiation.

Regardless of these few examples, the use of C–TiO_2 Kronos vlp 7000 as a photocatalyst in the degradation of pollutants is still scarcely discussed in the literature and, to the best of our knowledge, this material has not been previously investigated regarding ATZ degradation. Given that, in this work we compare the commercial materials TiO_2 P25 and C–TiO_2 Kronos vlp 7000 for removing ATZ in a tubular photochemical reactor coupled to a CPC irradiated by simulated sunlight. Reactors equipped with composite parabolic collectors (CPC) have the characteristic of providing high photodegradation rates due to their optimized photon harvesting geometry (Maffessoni et al. 2021; Malato et al. 2016), ensuring the illumination of the reactor tube by both direct and diffuse sunlight (Malato et al. 2016). These reactors have proven to be effective in treating water contaminated with pesticides (Colina-Márquez, Machuca-Martínez, and Li Puma 2009), estrogens (Colina-Márquez, Machuca-Martínez, and Li Puma 2015), antibiotics (Maffessoni et al. 2021), etc. However, studies using CPC solar reactors applied to ATZ degradation are still scarce. As an example, Arellano et al. (2013) achieved 68 % ATZ mineralization after 6 h of treatment in a CPC detoxification plant combining photo-Fenton with TiO_2-based photocatalysis in separate reactors.

Furthermore, considering that the comparison of these materials has not been deeply discussed in the literature, for the first time we compare the main characterization properties of TiO_2 P25 and C–TiO_2 Kronos vlp 7000, and analyze the changes in ATZ concentration over time in simulated sunlight in terms of degradation kinetic models and total organic carbon removal, in addition to elucidating the intermediates formed during photocatalysis in each case.

2 Materials and methods

2.1 Reagents and photocatalytic materials

Atrazine (technical grade ≥92 % w/w) was provided by Syngenta, and used with no further purification. The aqueous solutions were prepared in pure water (Milli-Q®, 18.2 MΩ cm). 1-mol L^{-1} H_2SO_4 (prepared from 98 % w/w H_2SO_4, Vetec) or 1-mol L^{-1} NaOH (prepared from NaOH 97 % w/w, Vetec) were used for pH correction. High performance liquid chromatography (HPLC) grade acetonitrile (J. T. Baker) and 100 % acetic acid (Merck) were used in the chromatographic analyses.

TiO_2 Aeroxide® P25 and C–TiO_2 Kronos® vlp 7000 were supplied by Evonick Degussa GmbH (Brazil) and Kronos International, Inc. (Germany), respectively.

2.2 Experimental apparatus

Figure 1 depicts the experimental apparatus used, which consisted in a tubular photochemical reactor coupled to a compound parabolic collector (CPC), operated in the recirculation batch mode. The reactor was a Duran® borosilicate glass tube (28.6 mm internal diameter, 2.0 mm thickness, 355 mm in length, and irradiated volume of 0.23 L). The collector was made of polished aluminum with the following characteristics: light intercept angle: 180°; optical separation: 1.4 mm; concentration factor: 1.0; and reflective surface: 0.04 m^2. The total volume of the solution used in all the experiments was 2 L and the recirculation flow rate was kept constant at 175 L h^{-1}. The circulation between the tank and the reactor was provided by a centrifugal pump (Bomax); the liquid flow rate was set using a needle valve and measured by a rotameter. Samples were taken from the piping connecting the reactor and the recirculation tank. The experiments were conducted at constant temperature (25 °C).

The reactor was irradiated by one Xenon arc lamp (set to 1000, 2000, 3000 and 4000 W) positioned 3 m above the reactor. The spectral distribution of the light on the surface of the CPC (Figure S1) was measured using a spectroradiometer (Luzchem SPR-4002), and is quite similar to that of the standard AM 1.5 solar spectrum (http://rredc.nrel.gov/solar/spectra/am1.5) in the range ~300–450 nm. The corresponding specific photon rate reaching the reactor was measured using standard ferrioxalate actinometry (Braun, Maurette, and Oliveros 1991), resulting in an average value of $(3.23 \pm 0.20) \times 10^{-5}$ E L^{-1} s^{-1} (see Supplementary Material for information on actinometry essays).

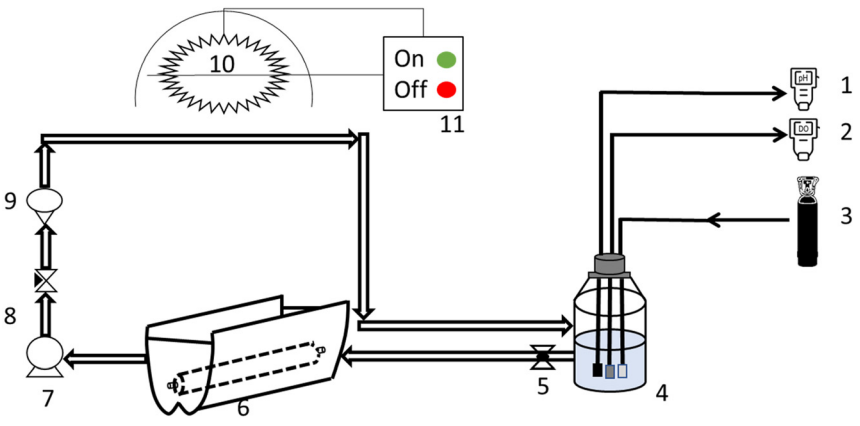

Figure 1: Simplified scheme of the experimental apparatus. 1 – pH meter; 2 – dissolved oxygen meter; 3 – oxygen cylinder (99.8 % purity); 4 – recirculation tank; 5 – discharge valve; 6 – tubular reactor coupled with CPC; 7 – centrifugal pump; 8 – needle valve; 9 – rotameter; 10 – light source; and 11 – lamp activation system.

2.3 Procedures

2.3.1 pKa: The pKa of aqueous atrazine was determined from seven aqueous solutions of the same concentration (5 mg L^{-1}) in duplicate, with pH values of 1, 1.5; 2; 3; 4; 5 and 7. The UV-visible absorption spectra were obtained for each solution using a Varian Cary 50 spectrophotometer. The pKa were obtained for the wavelengths of maximum absorption of protonated and deprotonated forms of ATZ.

2.3.2 Molar absorption coefficient: The molar absorption coefficient (ε) of aqueous ATZ in the wavelength range 200–340 nm was obtained from the angular coefficient of the absorbance curve as a function of concentration (1, 3, 5, 7, and 9 mg L^{-1}) for each wavelength, according to the Beer–Lambert law. The UV-visible absorption spectra were measured for each solution using a Varian Cary 50 spectrophotometer. The pH of the solutions was adjusted to 1, 3, or 7, the latter being the approximate natural pH of aqueous atrazine.

2.3.3 Atrazine hydrolysis and adsorption assays: Hydrolysis assays were performed in the absence of light in triplicate. With this aim, three amber flasks containing 30 mg L^{-1} ATZ solutions at 25 °C and selected pH (3, 5, 7, and 9) were kept in a thermostatic rotating incubator (Tecnal, model TE-421) set at 200 rpm. Samples were taken at times 0, 6, and 24 h to measure ATZ concentration.

Adsorption assays were performed at an initial ATZ concentration of 30 mg L^{-1}, varying only the content of TiO_2 P25 (100 mg L^{-1}) or C–TiO_2 Kronos vlp 7000 (500 mg L^{-1}). The aqueous suspension containing the herbicide and the catalyst (pH 6 for TiO_2 P25 and pH 7 for C–TiO_2 Kronos), was added to amber flasks kept in a rotating incubator (200 rpm, 25 °C) in the dark. Samples were taken at 0, 5, 10, 15, 30, 45, 60, 90, and 120 min, filtered through 0.22-μm diameter membrane filters, and analyzed by HPLC. This set of experiments was performed in triplicate.

2.3.4 Photolysis assays: ATZ photolysis was evaluated over 2 h, in the reactor depicted in Figure 1 under the following conditions: $[ATZ]_0$ = 30 mg L^{-1}; pH 6; dissolved oxygen (DO) concentration equal 8.5 mg L^{-1}; 25 °C. Samples were withdrawn at 0, 5, 10, 15, 30, 45, 60, 90, and 120 min, and analyzed by HPLC and TOC to quantify ATZ degradation and pollutant mineralization. These experiments were performed in duplicate.

2.3.5 Photocatalytic experiments: The reactor shown in Figure 1 was assembled for atrazine degradation experiments using TiO_2 P25 or C–TiO_2 Kronos vlp 7000. Initially, the aqueous suspension containing the herbicide and the photocatalyst was prepared by weighing ATZ and catalyst masses separately, which were then added to water and transferred to a 2-L volumetric flask. The later was kept in an ultrasonic bath (Fisher Scientific, model FS110) for 30 min. The solution pH was fixed at 6 for P25 and 7 for C–TiO_2 Kronos vlp 7000, for which the materials are not in their isoelectric points. After pH correction to the desired initial value, the suspension was transferred to the tank and recirculated for about 30 min. After 15 min, the initial sample was collected at time zero, and the reactor was exposed to simulated solar light. 1 mL samples were then collected at times 5, 10, 15, 30, 45, 60, 90, and 120 min, and analyzed by HPLC. During the experiments, oxygen (Air Liquide, 99.8 %) was continuously introduced into the recirculation tank through a porous diffuser to reach saturation at room temperature (8.5 mg L^{-1}); the dissolved oxygen concentration was measured using an Oakton equipment (DO 300 series). In our study, in addition to allowing direct quantification by high performance liquid chromatography (HPLC) without the need for pre-concentration steps, initial ATZ concentrations in the range of 1–30 mg L^{-1} were used to accurately elucidate degradation intermediates and quantify total organic carbon. This concentration range is typical of primary effluents from industrial production and/or formulation facilities, or also of rinse water generated in the agroindustry during washing of containers, spraying equipment or empty product bottles (Zhang and Pagilla 2010).

2.4 Analyses

2.4.1 Total organic carbon (TOC): The total organic carbon (TOC) was measured with a Shimadzu TOC-L equipment. The TOC corresponded to the difference between the total carbon (TC) and inorganic carbon (IC) concentrations of the solution.

2.4.2 High-performance liquid chromatography (HPLC): Atrazine concentrations were quantified by HPLC using a Shimadzu UFLC chromatograph equipped with a C18 Phenomenex column (250 mm × 4.60 mm, 5 μm) and a UV/VIS-SPD-10A detector. Isocratic conditions were used, with the mobile phase consisting of 50 % acetonitrile (phase B) and 50 % Milli-Q® water containing 0.2 % (v/v) acetic acid (phase A). The flow rate, oven temperature, injection volume, and detection wavelength were 1 mL min^{-1}, 40 °C, 50 μL, and 220 nm, respectively. At this wavelength, the measured molar absorption coefficient of ATZ is about 35,000 L mol^{-1} cm^{-1}. The limits of detection and quantitation were 0.025 and 0.075 mg L^{-1}, respectively. ATZ retention time was 9 min.

2.4.3 High-performance liquid chromatography coupled to mass spectrometry (LC-MS): The liquid chromatography (LC) system consisted of a Prominence equipment equipped with binary pumps (Shimadzu LC-20AD) and an autosampler (Shimadzu SIL 20AC). A C18 Shimpack XR-ODS column (30.0 mm × 2.0 mm, 2.2 μm) was used. The mobile phase contained (A) Milli-Q® water and (B) methanol; isocratic elution 50 % water/50 % methanol was used. The mobile phase flow rate and the injected sample volume were 0.2 mL min^{-1} and 5 μL, respectively. A LCMS-IT-TOF (Shimadzu) mass spectrometer coupled with the HPLC equipment was employed. The electrospray type-probe (ESI) operated in positive mode (4.5 kV). Nitrogen was used for sample drying, at a pressure of 100 kPa and flow rate of 1.5 L min^{-1}. The curved desolvation line (CDL) interface was set at 200 °C. The accumulation time of ions in the octupole was 10 ms. The mass spectra were obtained in the range 100–600 *m/z*. For the structural elucidation of particular compounds, selected ion monitoring experiments were carried out, with specific ion trap selection submitted to Argon (>99.99 %) collision (energy and concentration equal to 50 % of the maximum values).

2.5 Materials characterization

2.5.1 Diffuse reflectance spectroscopy: UV-visible diffuse reflectance spectra of the materials were obtained using a Shimadzu UV-2550 spectrophotometer coupled with an integrating sphere device. The reflectance spectra of TiO_2 P25 and C–TiO_2 Kronos vlp 7000 were obtained with 0.1 g of a diluted sample of each material in 1.5 g $BaSO_4$ (reference compound). The band gap energy was calculated using the Kubelka-Munk function Equation (1), as detailed by (Makuła, Pacia, and Macyk 2018).

$$F(R_\infty) = \frac{(1-R_\infty)^2}{2R_\infty} = \frac{K}{S} \quad (1)$$

In Equation (1), $F(R)$ is the reflectance of the sample; R is the reflection coefficient; K is the absorption constant; and S is the scattering coefficient (S ~1.10 for TiO_2 P25 and ~0.40 for C–TiO_2 Kronos vlp 7000).

2.5.2 X-ray diffraction: X-ray diffractograms were obtained in the range 2–90° (2θ) in a Philips X'Pert MPD model diffractometer, using copper Kα radiation with a step of 0.02° (2θ) at 1 s/step.

2.5.3 BET specific surface area: The specific surface area of the materials was determined from nitrogen adsorption data using BET isotherms (Brunauer, Emmett, and Teller 1938), in a Quantachrome equipment, model Nova 1000. The samples were previously degassed at 150 °C for 1 h. The cross-sectional area of the N_2 molecule was 16.2 $Å^2$ (Brown, Miron, and Fellows 2019).

2.5.4 Infrared spectroscopy (IR): The infrared spectra of the photocatalytic materials were obtained using a Fourier transform infrared spectrometer (model IRPrestige-21, Shimadzu) coupled to a Pike MIRacleTM attenuated full reflectance apparatus with germanium crystal sample holder. The spectra with a resolution of 2 cm^{-1} were acquired in the wavelength range 700–4000 cm^{-1}.

3 Results and discussion

3.1 Materials characterization

Figure 2 shows the diffractograms of the photocatalytic materials under study. The characteristic peaks of anatase and rutile are found at 2θ = 25.5 and 27.7°, respectively, which are peaks of highest intensity for each crystalline phase. The C–TiO_2 Kronos vlp 7000 material contains only anatase, which is in accordance with the manufacturer's information. The sizes of the crystallites of each material were calculated by the Scherrer equation (Lim, Marks, and Rowles 2020), resulting 19.8 nm (TiO_2 P25) and 13.9 nm (C–TiO_2 Kronos vlp 7000), which are close to the values informed by the manufactures (21 and 15 nm, respectively).

Figure 3 shows typical type-IV adsorption isotherms for both materials, revealing that capillary condensation occurred at relative pressures higher than 0.9 (Buttersack 2019). Above this value, the isotherm of TiO_2 P25 presents hysteresis similar to the H3 type (Figure 3A), with a sudden increase in the adsorbed volume for relative pressures between 0.9 and 1.0, suggesting the presence of mesopores and macropores. This mesoporous structure can facilitate contaminants molecules to diffuse within the solids during photocatalytic reactions. In turn, for C–TiO_2 Kronos vlp 7000, Figure 3B shows overlapping of the adsorption/desorption curves until P/P_0 of about 0.4, suggesting slit-like lamellar morphology. Above this value, the C–TiO_2 material shows hysteresis, probably indicating a more significant contribution of mesopores in the adsorption/desorption process. This fact can be seen in Table 1, as C–TiO_2 Kronos vlp 7000 had a smaller average pore diameter compared to that of TiO_2 P25. In this case, an increase in the adsorbed volume is observed for relative pressures in the range 0.4–1.0, suggesting the presence of both micro and mesopores.

The results of specific surface area, micropore volume, and mean pore diameter are summarized in Table 1; pore width distributions are shown in Figure S2, which clearly confirm the largest fraction of pores between 1 and 10 nm in the C–TiO_2 Kronos vlp 7000 material. The average pore diameters are 4.35 nm (TiO_2 P25) and 8.70 nm (C–TiO_2 Kronos vlp 7000), which are within the characteristic range 2–50 nm for mesoporous materials (Wen et al. 2020).

According to Manassero, Satuf, and Alfano (2013), the specific surface areas of TiO_2 P25 and C–TiO_2 Kronos vlp 7000 are approximately 50 and > 250 $m^2\,g^{-1}$, respectively. Berberidou et al. (2019) also provided information on the surface area of these materials. For TiO_2 P25 and Kronos vlp 7000, the BET surface areas were found as 55 ± 15 $m^2\,g^{-1}$ and

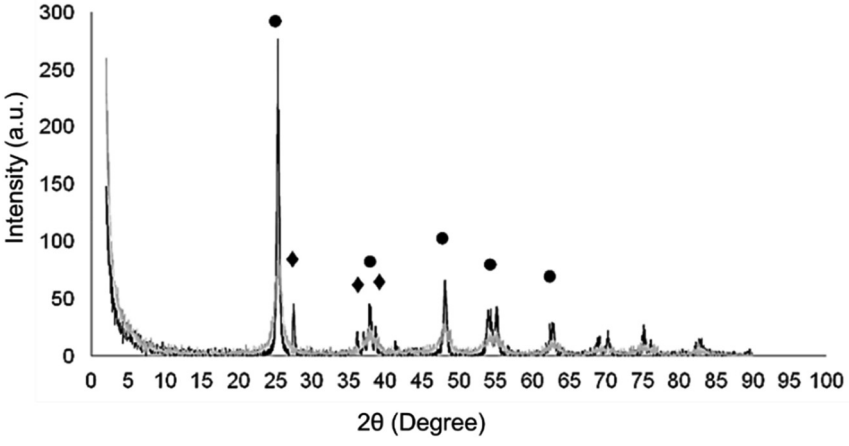

Figure 2: X-ray diffraction patterns of TiO_2 P25 (black curve) and C–TiO_2 Kronos vlp 7000 (grey curve). ● Anatase. ◆ Rutile.

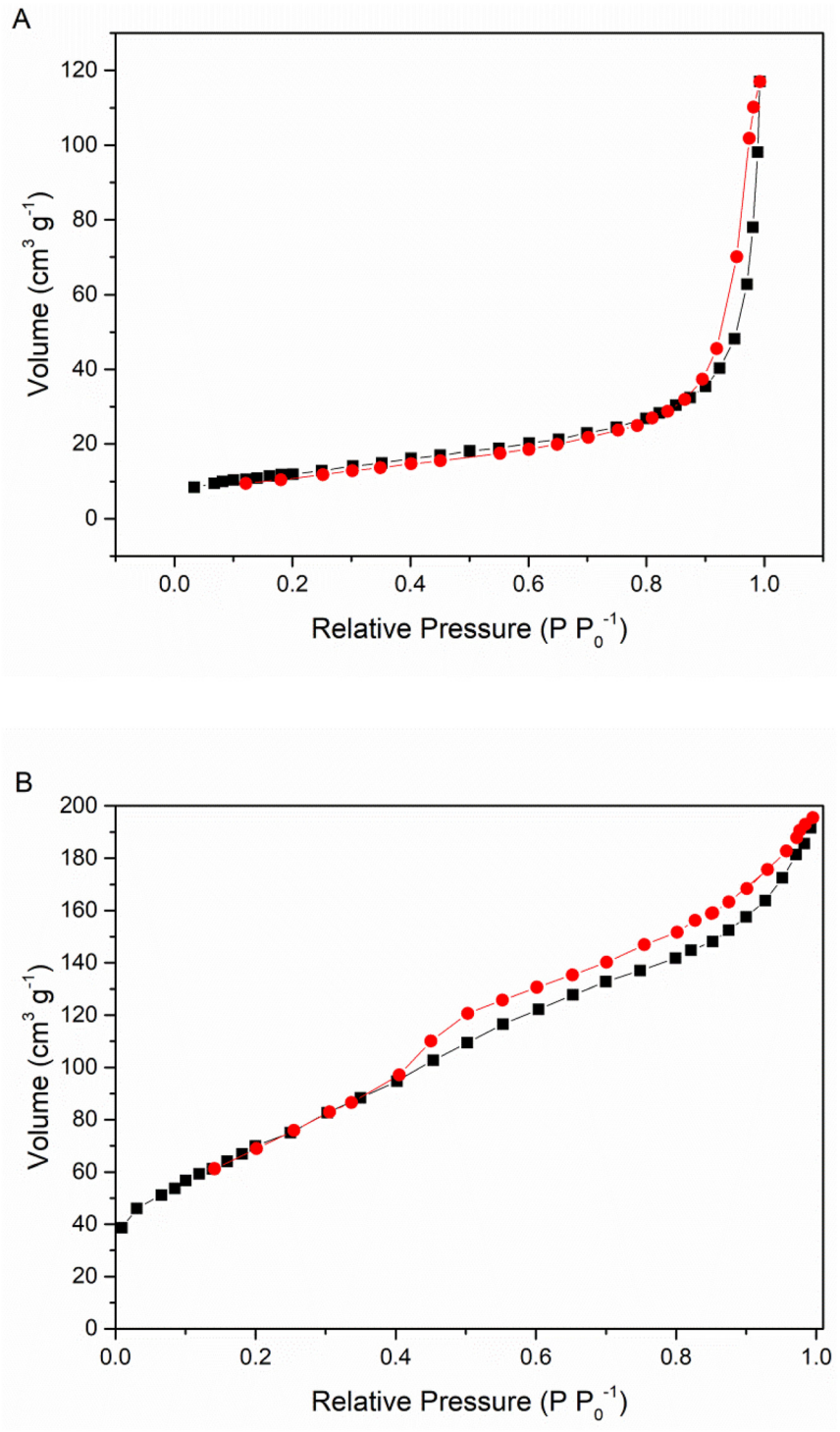

Figure 3: N_2 adsorption isotherms for (A) P25 TiO_2 and (B) C–TiO_2 Kronos vlp 7000, showing adsorption (■) and desorption (●).

>250 m^2 g^{-1}, respectively, which are consistent with ours. The high semiconductor surface area influences positively the heterogeneous photocatalysis process for C–TiO_2 Kronos vlp 7000. Nevertheless, the fact that TiO_2 P25 is composed of both anatase and rutile phases in the 80:20 ratio may contribute to reduce electron-hole recombination (Rambabu, Jaiswal, and Roy 2016).

The diffuse reflectance spectra and the results of the Kubelka-Munk calculations are shown in Figures S3–S5. The corresponding band gap energies were 3.42 eV (360 nm) and 3.22 eV (387 nm) for TiO_2 P25 and C–TiO_2 Kronos vlp 7000, respectively; these values are close to those reported by Khoa Le et al. (2015) and Berberidou et al. (2019), respectively. As a consequence, C–TiO_2 Kronos vlp 7000 should

Table 1: Main morphological parameters of TiO_2 P25 and C–TiO_2 Kronos vlp 7000.

Materials	BET surface area ($m^2\ g^{-1}$)	Micropore volume ($cm^3\ g^{-1}$)	Average pore diameter (nm)
TiO_2 P25	45.4 ± 0.1	0.099	8.70
C–TiO_2 Kronos vlp 7000	258.4 ± 1.5	0.281	4.35

perform better near the visible range. As a carbon-doped material, C–TiO_2 Kronos vlp 7000 is also expected to absorb in the visible light spectrum to some extent (λ > 400 nm). According to Berberidou et al. (2019), by replacing oxygen by carbon atoms, new energy states are generated in the TiO_2 band gap, making possible visible light absorption. However, as discussed in detail further on, none of the experiments showed superior performance of C–TiO_2 Kronos over TiO_2 P25. Berberidou et al. (2019) also found nearly negligible degradation of thiacloprid in the presence of TiO_2 Kronos vlp 7000 under visible irradiation. The lower performance of C–TiO_2 Kronos compared to TiO_2 P25 may be due to the non-substitution of oxygen by carbon atoms, which as mentioned earlier, is alleged to be responsible for generating new energy states for the carbon-modified catalyst band gap (Fotiou et al. 2016).

The infrared (IR) spectra of TiO_2 P25 and C–TiO_2 Kronos vlp 7000 (Figure 4) show two bands between 3000 and 4000 cm^{-1}, possibly related to the O–H group stretching, indicating water adsorbed on these materials. Bands at 600 cm^{-1} are also noticeable for both catalysts, indicating the presence of Ti–O stretching and Ti–O–Ti bridging stretching modes (Wang et al. 2012). In addition, the absorption bands

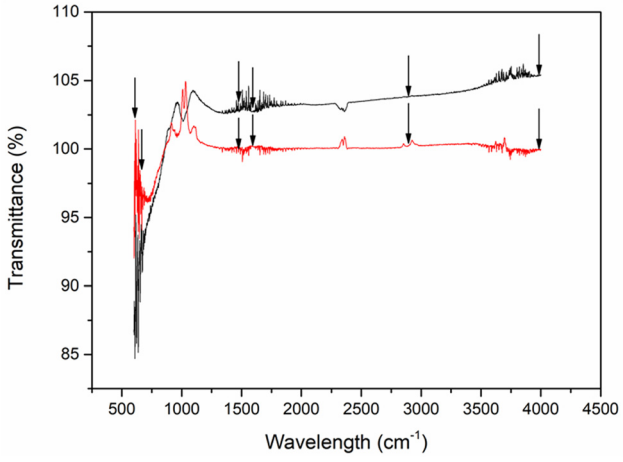

Figure 4: Infrared spectra of TiO_2 P25 (red) and C–TiO_2 Kronos vlp 7000 (black).

in the range 1550–1630 cm^{-1} for C–TiO_2 Kronos vlp 7000 suggest the presence of aryl carboxylate groups in this material. The aryl carboxylate functional group typically exhibits characteristic IR absorption bands in the 1700–1600 cm^{-1} range. Specifically, the carboxylate group (COO–) exhibits a strong peak around 1600 cm^{-1} due to the asymmetric stretching vibration of the COO– bond, and a weaker peak around 1400 cm^{-1} due to symmetric stretching of the COO– bond (Tanwar, Singh, and Sharma 2023). The aromatic ring ($C_6H_5^-$) typically exhibits absorption bands in the 1600–1500 cm^{-1} range due to C=C stretching vibrations (Mamedbeili et al. 2011; Volkov, Rogova, and Proskurnin 2021).

3.2 Control runs

Figure S6 reveals the existence of two isosbestic points at 210 and 241 nm; a pKa value of 1.75 was obtained for ATZ, which is close to the value (~1.7) reported in the literature (Mohammadi et al. 2019; Sun et al. 2019). pH values of 6 and 7 were then selected, so that aqueous atrazine molecules were completely in their neutral state. Control assays at pH 6 confirmed that no ATZ hydrolysis occurred over 24 h, as discussed in the literature (Prosen and Zupančič-Kralj 2005). Moreover, no appreciable ATZ removal by adsorption on the TiO_2 P25 and C–TiO_2 Kronos vlp 7000 materials was observed. Finally, approximately 18 % atrazine removal by photolysis was achieved after 120 min exposure to simulated solar light in the absence of catalysts ($[ATZ]_0$ = 30 mg L^{-1}; DO = 8.5 mg L^{-1}, pH 6). Accordingly, low atrazine removal (6.4 %, $[ATZ]_0$ = 100 µg L^{-1}) was reported (Komtchou et al. 2018) during 180 min irradiation under simulated direct solar light (100 mW cm^{-2}). Cheshme Khavar et al. (2018) achieved even lower ATZ removal by direct photolysis, which was below 5 % ($[ATZ]_0$ = 40 mg L^{-1}, pH = 5.4, 60 min).

3.3 Influence of catalysts concentration on atrazine degradation

Eight experiments were conducted, all in duplicate, using 2 L of a 30 mg L^{-1} ATZ solution containing 100, 200, 500 and 1000 mg L^{-1} of each catalyst. The initial pH was corrected to 6.0 for TiO_2 P25 and 7.0 for C–TiO_2 Kronos vlp 7000. The results are presented in Figure 5.

Figure 5A shows that 500 mg L^{-1} of TiO_2 P25 provided the best atrazine photodegradation at the end of 120 min (86 %), a result similar to that of Velegraki et al. (2015). In contrast, the use of 100 mg L^{-1} of the C–TiO_2 Kronos vlp 7000 material resulted in the best ATZ degradation (37 %) degradation after 120 min (Figure 5B). Interestingly, as the concentration of

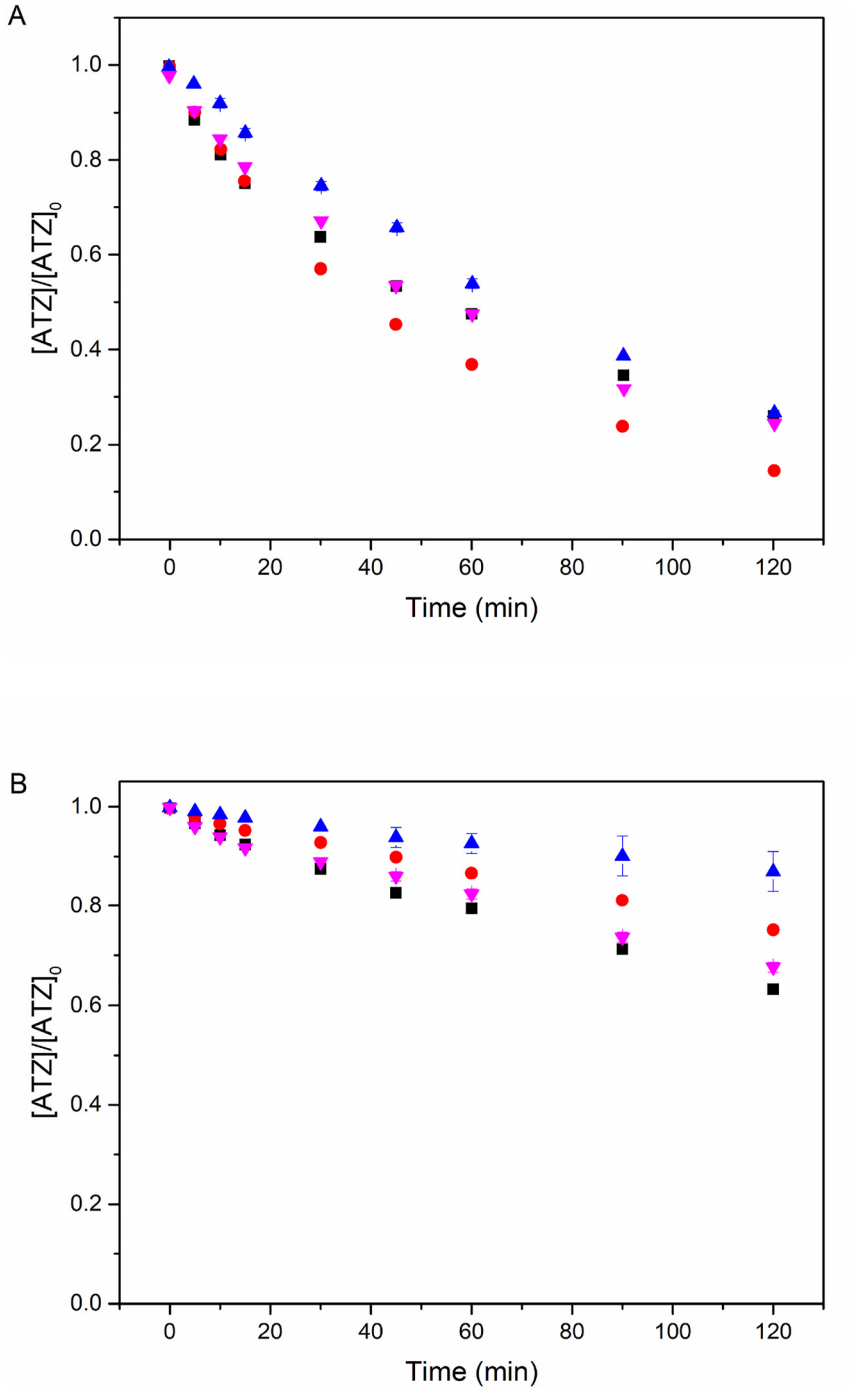

Figure 5: Influence of catalyst concentration on atrazine ([ATZ]$_0$ = 30 mg L^{-1}) degradation. (A) TiO_2 P25; (B) C–TiO_2 Kronos vlp 7000. ■ 100 mg L^{-1}; ▼ 200 mg L^{-1}; ● 500 mg L^{-1}; ▲ 1000 mg L^{-1}.

this material was reduced from 1000 to 100 mg L^{-1}, an increase in ATZ degradation could be observed. This is in good agreement with Jebaranjitham and Kumar (2020), who mentioned that at higher catalyst concentrations, unsuitable light scattering or photon-blocking due to turbidity may interfere in a wide range of UV wavelengths, therefore affecting the degradation efficiency. Other consequences of using high catalyst content include particle agglomeration, thus reducing the available surface area and the number of surface-active sites, decreasing the photodegradation efficiency as a consequence. This may have occurred for C–TiO_2 Kronos vlp 7000, as it was not as efficient in removing atrazine when compared to TiO_2 P25. Furthermore, the low ATZ removal and mineralization observed may also be associated with blocking of active sites by intermediate compounds formed from the herbicide degradation, which may also have exhibited a recalcitrant character (Oturan, Brillas, and Oturan 2012).

3.4 Kinetic study

Five atrazine degradation experiments were performed in duplicate. TiO_2 P25 concentration was kept at 500 mg L^{-1} (Figure S7). The results indicate significant ATZ degradation after 120 min, with 100 %; 98 %; 98 %; 93 and 86 % removals for $[ATZ]_0$ = 1.2; 4.9; 11.1; 20.1 and 29.8 mg L^{-1}, respectively. Moreover, the results depicted in Figure 6A reveal that the initial ATZ degradation rate, calculated from the concentration-time curves, increased with $[ATZ]_0$ up to 20 mg L^{-1} and then decreased.

In fact, the competition between ATZ and the degradation products adsorbed on the catalyst particles surface, particularly at higher initial herbicide concentration, may limit the photocatalyst performance. Berberidou et al. (2019) also found that by increasing TiO_2 concentration, the photodegradation performance is diminished. An important condition is the suspension of catalyst particles, which can

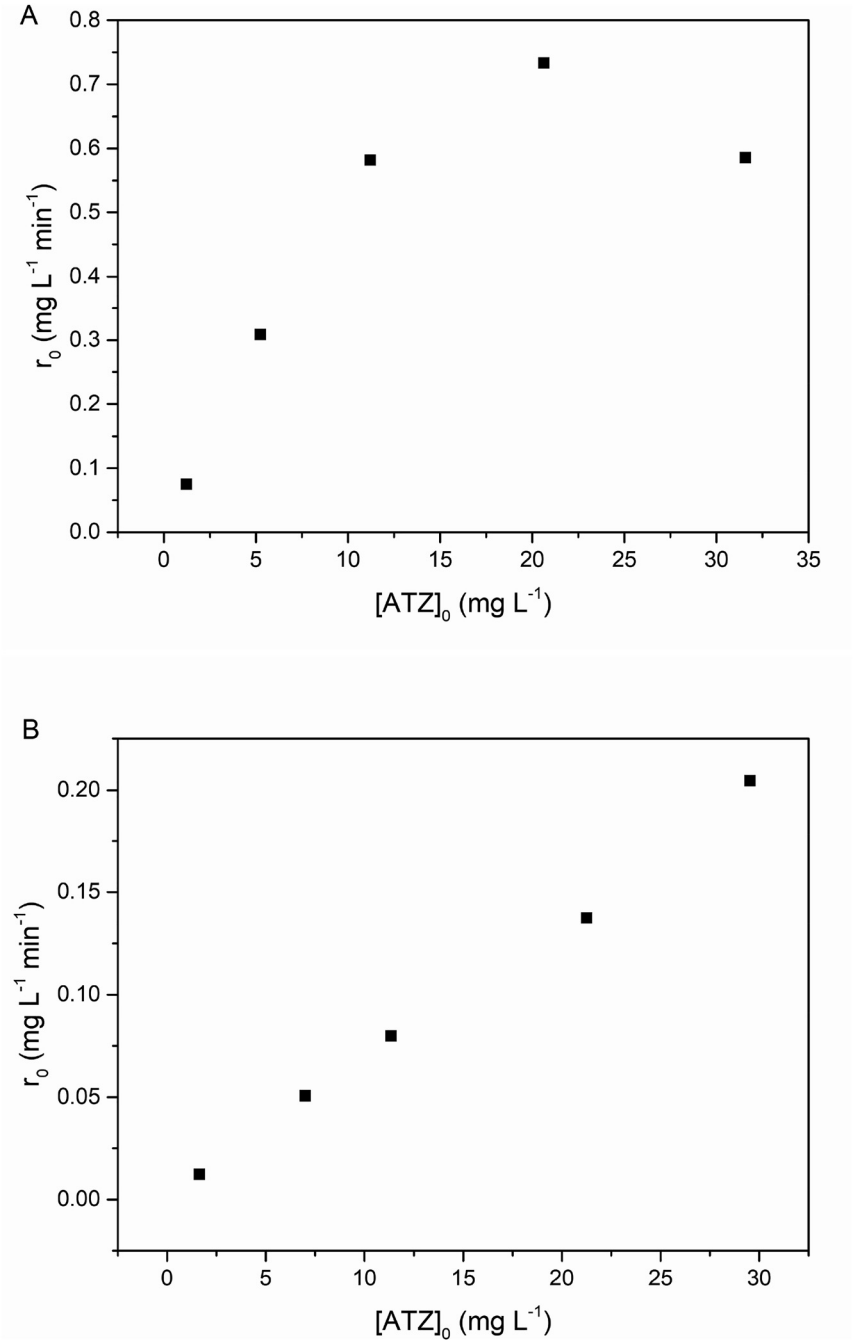

Figure 6: Dependence of the initial degradation rate (r_0) with initial ATZ concentration for (A) TiO_2 P25 (500 mg L^{-1}; pH = 6; 25 °C) and (B) C–TiO_2 Kronos vlp 700 (100 mg L^{-1}; 100 mg L^{-1}; pH = 7; 25 °C).

affect the penetration of UV irradiation, enhancing light scattering. Another nonpareil situation is the particle-particle interactions that can hamper the surface area available for light absorption.

Moreover, ATZ at higher initial concentrations may compete with the photocatalyst for incident UV-visible radiation, resulting in reduced efficiency of the photocatalytic reaction due to the decreased concentration of the HO• radicals formed (Daneshvar et al. 2007; Grzechulska and Morawski 2002; So et al. 2002; Tang, An, and Huren 1995). Nevertheless, according to Marchetti et al. 2013, there is limited absorption of sunlight by ATZ, with $\varepsilon_{ATZ}^{300\,nm} \sim 300\ L\ mol^{-1}\ cm^{-1}$ and $\varepsilon_{ATZ}^{320\,nm} \sim 100\ L\ mol^{-1}\ cm^{-1}$.

The data in Figure S8 was used to estimate the parameters of the Langmuir-Hinshelwood (LH) kinetic model Eq. (2) (Kumar, Porkodi, and Rocha 2008):

$$r_0 = \frac{K_r K_{ads} C_{ATZ,0}}{1 + K_{ads} C_{ATZ,0}} \quad (2)$$

where K_r is the reaction rate constant and K_{ads} is the ATZ adsorption constant onto TiO_2 particles; the resulting values are $1.57\ mg\ L^{-1}\ min^{-1}$ and $0.041\ L\ mg^{-1}$, respectively (see Figure S8). While this simplified approach obviously excludes the contribution of direct herbicide photolysis, as discussed previously, it is useful for comparison with the other semiconductor investigated in this study.

The same procedure was repeated for C–TiO_2 Kronos vlp 700 ($100\ mg\ L^{-1}$), varying the initial ATZ concentration at the same levels (Figure S9). In this case, ATZ removals of 37 %; 35 %; 38 %; 39 and 45 % were obtained after 120 min, for $[ATZ]_0$ = 1.7; 7.0; 11.4; 21.3 and $29.5\ mg\ L^{-1}$, respectively. Figure 6B shows that the estimated initial degradations rates increased linearly with $[ATZ]_0$. In fact, since the C–TiO_2 Kronos material has a larger surface area, there should be no saturation of its surface sites by ATZ molecules and degradation products (formed in smaller quantities). On the other hand, in addition to the absence of the heterojunction structure involving anatase and rutile in TiO_2 P25, the charge recombination rate in C–TiO_2 Kronos vlp 7000 was reported to be higher compared with TiO_2 P25 (Fotiou et al. 2016), which could explain the low ATZ removals obtained. In this case, the calculated values of K_r and K_{ads} of the LH model were $1.30\ mg\ L^{-1}\ min^{-1}$ and $0.0057\ L\ mg^{-1}$, respectively (Figure S10). Interestingly, although the K_r value is very close to that obtained for the TiO_2 P25 photocatalyst ($1.57\ mg\ L^{-1}\ min^{-1}$), the K_{ads} value for C–TiO_2 Kronos vlp 7000 is almost ten times lower, which can be associated with the substantially larger specific surface area (258.4 and $45.4\ m^2\ g^{-1}$ for C–TiO_2 Kronos and TiO_2 P25, respectively). Considering the hypothesis that the contribution of direct photolysis to herbicide degradation is similar, regardless of the photocatalytic material used, it can be said that the LH model is a good approximation for atrazine degradation for both semiconductor materials.

3.5 Identification of degradation intermediates

Possible persistent intermediate compounds were identified as suggested by the chromatographic analysis during the study of atrazine degradation by means of the TiO_2 P25 catalyst (Figure S11). For this purpose, the mass spectrum of a sample collected at the end of two hours was obtained ($[ATZ]_0$ = $30\ mg\ L^{-1}$). The results are highlighted in Figures S12–S14, in which three intermediate compounds were identified: 2-chloro-4-acetamido-6-isopropylamino-1,3,5-triazine ($C_6H_{10}ClN_5$, m/z = 230.0790), with an elution time of 3.315 min; 2-chloro-4-ethylamino-6-amino-1,3,5-triazine ($C_5H_9ClN_5$, m/z = 174.0546), with an elution time of 1.325 min; and 2-hydroxy-4-acetamido-6-isopropylamino-1,3,5-triazine ($C_8H_{15}N_5O$, m/z = 212.1139), with an elution time of 0.995 min. Coelho and Bernardo (2017) and Hollanda et al. (2019) also reported the same intermediates in the degradation of ATZ by ozonation and zero-valent metals, respectively. In our work, ATZ mineralization by TiO_2 P25 was not significant during the experiments (<20 %, after 120 min). Hollanda et al. (2019) also found no mineralization of ATZ, even after its total disappearance. According to the authors, the reason is the generation of such persistent organic compounds.

In the case of the experiments using C–TiO_2 Kronos vlp 7000, the mass spectrum of a sample collected at the end of two hours was obtained ($[ATZ]_0$ = $30\ mg\ L^{-1}$) (Figure S15). Two intermediates could be identified: 2-hydroxy-4-isopropylamino-6-amino-s-triazine ($C_6H_{11}N_5O$, m/z = 169.9739) and 2-hydroxy-4-acetamindo-6-isopropylamino-s-triazine ($C_8H_{15}N_5O$, m/z = 211.0440), with elution times of 1.163 and 0.995 min, respectively. Chan and Chu (2005) and Chen et al. (2009) also reported in their works these intermediates with the use of the Fenton's oxidation and photolysis, respectively. 2-hydroxy-4-acetamindo-6-isopropylamino-s-triazine was also found by Li and Zhou (2019) for the catalytic oxidation of ATZ in the presence of iron scraps. It is noteworthy that no chlorinated intermediate was identified in the experiments performed with C–TiO_2 Kronos vlp 7000. Likewise, ATZ mineralization was less than 38 % over 120 min during the photocatalytic experiments performed with this material.

4 Conclusions

In this study, the properties and efficiency of TiO_2 P25 and TiO_2 modified with carbon (C–TiO_2 Kronos vlp 7000) used as photocatalysts were compared in the degradation of aqueous atrazine (ATZ).

As revealed by X-ray diffraction, and in comparison with TiO_2 P25, which contains anatase and rutile phases, C–TiO_2 Kronos vlp 7000 shows only anatase. The average crystallite sizes found for these materials were 19.8 and 13.9 nm, respectively, and the corresponding specific surface areas as determined by BET analyses were 45.4 and 258.4 $m^2 g^{-1}$, respectively. Typical type-IV adsorption isotherms were found for both materials, while TiO_2 P25 exhibited H3-type hysteresis with the presence of mesopores and macropores, and C–TiO_2 Kronos vlp 7000 was characterized by a slit-like lamellar morphology with a smaller average pore diameter and a more significant contribution of mesopores. The band gap energies were 3.42 and 3.22 eV for TiO_2 P25 and C–TiO_2 Kronos vlp 7000, respectively. Also, the absorption ranges in the interval of 1550–1630 cm^{-1}, as indicated by IR spectroscopy suggests the existence of aryl carboxylate groups in C–TiO_2 Kronos vlp 7000. In fact, this carbon-doped material is expected to absorb visible light to some extent in comparison with TiO_2 P25.

For TiO_2 P25, increased ATZ degradation was observed with increased catalyst concentration up to 500 mg L^{-1}; in contrast, an increase in ATZ degradation was observed as the concentration of C–TiO_2 Kronos vlp 7000 decreased from 1000 to 100 mg L^{-1}. ATZ removals in the range 86–100 % were obtained after 120 min of photocatalytic treatment with TiO_2 P25 (500 mg L^{-1}) under simulated solar radiation, for $[ATZ]_0$ varying in the range 29.8–1.2 mg L^{-1}, respectively. In contrast, the use of 100 mg L^{-1} of C–TiO_2 Kronos vlp 7000 resulted in removals of only 37–45 % over the same irradiation time. The kinetic study also revealed that for TiO_2 P25, the initial ATZ degradation rate increased with $[ATZ]_0$ up to 20 mg L^{-1} and then decreased, while the degradation rates increased linearly with the initial herbicide concentration for C–TiO_2 Kronos vlp 7000, which may be associated with its larger surface area. Excluding the contribution of direct herbicide photolysis (only ~18 % removal), the Langmuir-Hinshelwood kinetic model adequately fitted to ATZ degradation data for both materials. Finally, low ATZ mineralization was observed for the materials studied, with values below 20 and 38 % at the end of 120 min for TiO_2 P25 and C–TiO_2 Kronos vlp 7000, respectively. Given that, the main intermediate compounds formed were identified, and no chlorinated compounds were found when C–TiO_2 Kronos vlp 7000 was used.

Acknowledgments: The authors thank the Coordination for the Improvement of Higher Education Personnel (CAPES) - Brazil – Finance Code 001, and the National Council for Scientific and Technological Development (CNPq, Brazil, grant #311230/2020-2). We are also thankful to the Environmental Chemistry Research Group (GPQA/IQ-USP) and to Dr. Thiago Hewer for the support with the analysis of diffuse reflectance, and also to the Laboratory of Particulate Materials and Non-Metallic Solids (LMPSol/PMT-EPUSP) for the BET and X-ray diffraction analyses.

Author contributions: All the authors have accepted responsibility for the entire content of this submitted manuscript and approved submission.

Research funding: This work was funded by the Coordination for the Improvement of Higher Education Personnel (CAPES) – Brazil – Finance Code 001, and the National Council for Scientific and Technological Development (CNPq, Brazil).

Conflict of interest statement: The authors report there are no competing interests to declare.

Data availability statement: The data supporting the findings of this study are available within the article and its supplementary materials.

References

Al-Rasheed, R. A. 2005. “Water Treatment by Heterogeneous Photocatalysis an Overview.” In *4th SWCC Acquired Experience Symposium Held in Jeddah*, 1–14.

Arellano, C. A. P., A. J. González, S. S. Martínez, I. Salgado-Tránsito, C. P. Franco, C. A. Pineda Arellano, A. J. González, S. S. Martínez, I. Salgado-Tránsito, and C. P. Franco. 2013. “Enhanced Mineralization of Atrazine by Means of Photodegradation Processes Using Solar Energy at Pilot Plant Scale.” *Journal of Photochemistry and Photobiology A: Chemistry* 272: 21–7.

Berberidou, C., V. Kitsiou, D. A. Lambropoulou, D. Michailidou, A. Kouras, and I. Poulios. 2019. “Decomposition and Detoxification of the Insecticide Thiacloprid by TiO 2-mediated Photocatalysis: Kinetics, Intermediate Products and Transformation Pathways.” *Journal of Chemical Technology and Biotechnology* 94 (8): 2475–86.

Bonansea, R. I., M. V. Amé, and D. A. Wunderlin. 2013. “Determination of Priority Pesticides in Water Samples Combining SPE and SPME Coupled to GC–MS. A Case Study: Suquía River Basin (Argentina).” *Chemosphere* 90 (6): 1860–9.

Braun, A. M., M.-T. Maurette, and E. Oliveros. 1991. *Photochemical Technology*. Chichester, United Kingdom: John Wiley & Son Ltd.

Brown, T. C., D. J. Miron, and C. M. Fellows. 2019. “Pressure-varying Langmuir Parameters and Stepped Nitrogen Adsorption on Alumina and Silica.” *Physical Chemistry Chemical Physics* 21 (5): 2558–66.

Brunauer, S., P. H. Emmett, and E. Teller. 1938. “Adsorption of Gases in Multimolecular Layers.” *Journal of the American Chemical Society* 60 (2): 309–19.

Buttersack, C. 2019. “Modeling of Type IV and V Sigmoidal Adsorption Isotherms.” *Physical Chemistry Chemical Physics* 21 (10): 5614–26.

Cai, G., M. Ding, Q. Wu, and H.-L. Jiang. 2020. "Encapsulating Soluble Active Species into Hollow Crystalline Porous Capsules beyond Integration of Homogeneous and Heterogeneous Catalysis." *National Science Review* 7 (1): 37–45.

Chan, K. H. H., and W. Chu. 2005. "Model Applications and Mechanism Study on the Degradation of Atrazine by Fenton's System." *Journal of Hazardous Materials* 118 (1–3): 227–37.

Chen, C., S. Yang, Y. Guo, C. Sun, C. Gu, and B. Xu. 2009. "Photolytic Destruction of Endocrine Disruptor Atrazine in Aqueous Solution under UV Irradiation: Products and Pathways." *Journal of Hazardous Materials* 172 (2–3): 675–84.

Cheshme Khavar, A. H., G. Moussavi, A. R. Mahjoub, and M. Satari. 2018. "Facile Preparation of Multi-Doped TiO2/rGO Cross-Linked 3D Aerogel (GaNF@TGA) Nanocomposite as an Efficient Visible-Light Activated Catalyst for Photocatalytic Oxidation and Detoxification of Atrazine." *Solar Energy* 173: 848–60.

Cheshme Khavar, A. H., G. Moussavi, K. Yaghmaeian, A. R. Mahjoub, N. Khedri, M. Dusek, T. Vaclavu, and M. Hosseini. 2020. "A New Ru(Ii) Polypyridyl Complex as an Efficient Photosensitizer for Enhancing the Visible-Light-Driven Photocatalytic Activity of a TiO_2/reduced Graphene Oxide Nanocomposite for the Degradation of Atrazine: DFT and Mechanism Ins." *RSC Advances* 10 (38): 22500–14.

Coelho, E. R. C., and L. D. Bernardo. 2017. "The Presence and the Removal of Atrazine, Deethylatrazine, Deisopropylatrazine and Deethylhidroxiatrazine in a Pilot Plant Consisted of Ozonation and Slow Sand Filtration." *Engenharia Sanitária e Ambiental* 22 (4): 789–96.

Colina-Márquez, J., F. Machuca-Martínez, and G. Li Puma. 2015. "Modeling the Photocatalytic Mineralization in Water of Commercial Formulation of Estrogens 17-β Estradiol (E2) and Nomegestrol Acetate in Contraceptive Pills in a Solar Powered Compound Parabolic Collector." *Molecules* 20 (7): 13354–73.

Colina-Márquez, J., F. Machuca-Martínez, and G. Li Puma. 2009. "Photocatalytic Mineralization of Commercial Herbicides in a Pilot-Scale Solar CPC Reactor: Photoreactor Modeling and Reaction Kinetics Constants Independent of Radiation Field." *Environmental Science and Technology* 43 (23): 8953–60.

Conama, R. 2005. *357/2005. Dispõe Sobre a Classificação Dos Corpos de Água e Diretrizes Ambientais Para o Seu Enquadramento, Bem Como Estabelece as Condições e Padrões de Lançamento de Efluentes, e Dá Outras Providências*. Brasília: Official Diary of the Union.

Cruz, M., C. Gomez, C. J. Duran-Valle, L. M. Pastrana-Martínez, J. L. Faria, A. M. T. Silva, M. Faraldos, and A. Bahamonde. 2017. "Bare TiO 2 and Graphene Oxide TiO 2 Photocatalysts on the Degradation of Selected Pesticides and Influence of the Water Matrix." *Applied Surface Science* 416: 1013–21.

Daneshvar, N., M. A. A. Behnajady, Y. Zorriyeh Asghar, and Y. Z. Asghar. 2007. "Photooxidative Degradation of 4-nitrophenol (4-NP) in UV/H2O2 Process: Influence of Operational Parameters and Reaction Mechanism." *Journal of Hazardous Materials* 139 (2): 275–9.

de Albuquerque, F. P., J. L. de Oliveira, V. Moschini-Carlos, and L. F. Fraceto. 2020. "An Overview of the Potential Impacts of Atrazine in Aquatic Environments: Perspectives for Tailored Solutions Based on Nanotechnology." *The Science of the Total Environment* 700: 134868.

de Araujo, L. G., E. S. P. Prado, F. De Souza Miranda, R. Vicente, A. S. Da Silva Sobrinho, G. P. Filho, and J. T. Marumo. 2020a. "Physicochemical Modifications of Radioactive Oil Sludge by Ozone Treatment." *Journal of Environmental Chemical Engineering* 8 (5): 104128.

de Araujo, L. G., L. Oscar Conte, A. Violeta Schenone, O. M. Alfano, and A. C. S. C. Teixeira. 2020b. "Degradation of Bisphenol A by the UV/H2O2 Process: A Kinetic Study." *Environmental Science and Pollution Research* 27 (7): 7299–308.

EPA. 2009. "National Primary Drinking Water Regulations." In *Arsenic and Clarifications to Compliance and New Source Contaminants Monitoring*. U. S: United States Environmental Protection Agency.

Fotiou, T., T. M. Triantis, T. Kaloudis, K. E. O'Shea, D. D. Dionysiou, and A. Hiskia. 2016. "Assessment of the Roles of Reactive Oxygen Species in the UV and Visible Light Photocatalytic Degradation of Cyanotoxins and Water Taste and Odor Compounds Using C–TiO2." *Water Research* 90: 52–61.

Gani, K. M., and A. A. Kazmi. 2016. "Phthalate Contamination in Aquatic Environment: A Critical Review of the Process Factors that Influence Their Removal in Conventional and Advanced Wastewater Treatment." *Critical Reviews in Environmental Science and Technology* 46 (17): 1402–39.

Grzechulska, J., and A. W. Morawski. 2002. "Photocatalytic Decomposition of Azo-Dye Acid Black 1 in Water over Modified Titanium Dioxide." *Applied Catalysis B: Environmental* 36 (1): 45–51.

Hollanda, L. R., C. A. L. Graça, L. M. Andrade, M. A. Mendes, O. Chiavone-Filho, and A. C. S. C. Teixeira. 2019. "Non-traditional Atrazine Degradation Induced by Zero-Valent-Copper: Process Optimization by the Doehlert Experimental Design, Intermediates Detection and Toxicity Assessment." *Journal of Chemical Technology and Biotechnology* 94 (4): 1156–64.

Jebaranjitham, J. N., and B. G. Kumar. 2020. "Heterogeneous Type-I and Type-II Catalysts for the Degradation of Pollutants." In *Green Photocatalysts*, 209–34. Cham, Switzerland: Springer.

Khoa Le, T., D. Flahaut, H. Martinez, H. K. Hung Nguyen, and T. K. Xuan Huynh. 2015. "Study of the Effects of Surface Modification by Thermal Shock Method on Photocatalytic Activity of TiO2 P25." *Applied Catalysis B: Environmental* 165: 260–8.

Kitsiou, V., G. A. Zachariadis, D. A. Lambropoulou, D. Tsiplakides, and I. Poulios. 2018. "Mineralization of the Antineoplastic Drug Carboplatin by Heterogeneous Photocatalysis with Simultaneous Synthesis of Platinum-Modified TiO2 Catalysts." *Journal of Environmental Chemical Engineering* 6 (2): 2409–16.

Komtchou, S., N. Delegan, A. Dirany, P. Drogui, D. Robert, and M. A. El Khakani. 2018. "Removal of Atrazine by Photoelectrocatalytic Process under Sunlight Using WN-Codoped TiO2 Photoanode." *Journal of Applied Electrochemistry* 48 (12): 1353–61.

Komtchou, S., N. Delegan, A. Dirany, P. Drogui, D. Robert, and M. A. El Khakani. 2020. "Photo-electrocatalytic Oxidation of Atrazine Using Sputtured Deposited TiO2: WN Photoanodes under UV/visible Light." *Catalysis Today* 340: 323–33.

Kumar, K. V., K. Porkodi, and F. Rocha. 2008. "Langmuir–Hinshelwood Kinetics – A Theoretical Study." *Catalysis Communications* 9 (1): 82–4.

Lee, C. M., P. Palaniandy, and I. Dahlan. 2017. "Pharmaceutical Residues in Aquatic Environment and Water Remediation by TiO2 Heterogeneous Photocatalysis: A Review." *Environmental Earth Sciences* 76 (17): 611.

Li, H., and B. Zhou. 2019. "Degradation of Atrazine by Catalytic Ozonation in the Presence of Iron Scraps: Performance, Transformation Pathway, and Acute Toxicity." *Journal of Environmental Science and Health, Part B* 54 (5): 432–40.

Lim, D. J., N. A. Marks, and M. R. Rowles. 2020. "Universal Scherrer Equation for Graphene Fragments." *Carbon* 162: 475–80.

Maffessoni, D., I. C. Grazziotin, C. R. Klauck, T. Benvenuti, S. W. da Silva, and A. Meneguzzi. 2021. "Heterogeneous Photocatalysis of Moxifloxacin at a Pilot Solar Compound Parabolic Collector: Elimination of the Genotoxicity." *Journal of Environmental Management* 297: 113296.

Makuła, P., M. Pacia, and W. Macyk. 2018. "How to Correctly Determine the Band Gap Energy of Modified Semiconductor Photocatalysts Based on UV–Vis Spectra." *The Journal of Physical Chemistry Letters* 9 (23): 6814–7.

Malato, S., M. I. Maldonado, P. Fernández-Ibáñez, I. Oller, I. Polo, and R. Sánchez-Moreno. 2016. "Decontamination and disinfection of water by solar photocatalysis: The pilot plants of the Plataforma Solar de Almeria." *Materials Science in Semiconductor Processing* 42: 15–23.

Mamedbeili, E. G., I. A. Dzhafarov, K. A. Kochetkov, T. G. Kyazimova, K. I. Gasanov, and S. T. Alieva. 2011. "Synthesis of 2-Aminomethoxy-1-Benzylsulfanylpentanes." *Russian Journal of Organic Chemistry* 47 (6): 842–4.

Manassero, A., M. L. Satuf, and O. M. Alfano. 2013. "Evaluation of UV and Visible Light Activity of TiO2 Catalysts for Water Remediation." *Chemical Engineering Journal* 225: 378–86.

Marchetti, G., M. Minella, V. Maurino, C. Minero, and D. Vione. 2013. "Photochemical Transformation of Atrazine and Formation of Photointermediates under Conditions Relevant to Sunlit Surface Waters: Laboratory Measures and Modelling." *Water Research* 47 (16): 6211–22.

Mohammadi, F., A. Esrafili, M. Kermani, M. Farzadkia, M. Gholami, and M. Behbahani. 2019. "Application of Amino Modified Mesostructured Cellular Foam as an Efficient Mesoporous Sorbent for Dispersive Solid-phase Extraction of Atrazine from Environmental Water Samples." *Microchemical Journal* 146: 753–62.

Mukimin, A., H. Vistanty, and N. Zen. 2020. "Hybrid Advanced Oxidation Process (HAOP) as Highly Efficient and Powerful Treatment for Complete Demineralization of Antibiotics." *Separation and Purification Technology* 241: 116728.

No. 2001. "The European Parliament and of the Council of 20 November 2001 Establishing the List of Priority Substances in the Field of Water Policy and Amending Directive 2000/60/EC." *Official Journal of the European Communities* 15: 1–5.

Ong, C. B., L. Y. Ng, and A. W. Mohammad. 2018. "A Review of ZnO Nanoparticles as Solar Photocatalysts: Synthesis, Mechanisms and Applications." *Renewable and Sustainable Energy Reviews* 81: 536–51.

Oturan, N., E. Brillas, and M. A. Oturan. 2012. "Unprecedented Total Mineralization of Atrazine and Cyanuric Acid by Anodic Oxidation and Electro-Fenton with a Boron-Doped Diamond Anode." *Environmental Chemistry Letters* 10 (2): 165–70.

Prosen, H., and L. Zupančič-Kralj. 2005. "Evaluation of Photolysis and Hydrolysis of Atrazine and its First Degradation Products in the Presence of Humic Acids." *Environmental Pollution* 133 (3): 517–29.

Rambabu, Y., M. Jaiswal, and S. C. Roy. 2016. "Probing the Charge Recombination in rGO Decorated Mixed Phase (Anatase-rutile) TiO2 Multi-Leg Nanotubes." *AIP Advances* 6 (11): 115010.

Romão, J., G. Mul. 2016. "Substrate Specificity in Photocatalytic Degradation of Mixtures of Organic Contaminants in Water." *ACS Catalysis* 6 (2): 1254–62.

Serrano-Martínez, A., M. T. Mercader-Ros, I. Martínez-Alcalá, C. Lucas-Abellán, J. A. Gabaldón, and V. M. Gómez-López. 2020. "Degradation and Toxicity Evaluation of Azo Dye Direct Red 83:1 by an Advanced Oxidation Process Driven by Pulsed Light." *Journal of Water Process Engineering* 37: 101530.

Singh, S., V. Kumar, N. Upadhyay, and J. Singh. 2020. "The Effects of Fe(II), Cu(II) and Humic Acid on Biodegradation of Atrazine." *Journal of Environmental Chemical Engineering* 8 (2): 103539.

So, C. M., M. Y. Cheng, J. C. Yu, and P. K. Wong. 2002. "Degradation of Azo Dye Procion Red MX-5B by Photocatalytic Oxidation." *Chemosphere* 46 (6): 905–12.

Spasiano, D., R. Marotta, S. Malato, P. Fernandez-Ibanez, and I. Di Somma. 2015. "Solar Photocatalysis: Materials, Reactors, Some Commercial, and Pre-industrialized Applications. A Comprehensive Approach." *Applied Catalysis B: Environmental* 170–171: 90–123.

Spyrou, A., A. Tzamaria, M. Dormousoglou, A. Skourti, D. Vlastos, M. Papadaki, and M. Antonopoulou. 2022. "The Overall Assessment of Simultaneous Photocatalytic Degradation of Cimetidine and Amisulpride by Using Chemical and Genotoxicological Approaches." *The Science of the Total Environment* 838: 156140.

Sun, J., X. Ma, W. Wang, J. Zhang, H. Zhang, Y. Wang, and J. Feng. 2019. "The Adsorption Behavior of Atrazine in Common Soils in Northeast China." *Bulletin of Environmental Contamination and Toxicology* 103 (2): 316–22.

Suri, R. P. S., J. Liu, D. W. Hand, J. C. Crittenden, D. L. Perram, and M. E. Mullins. 1993. "Heterogeneous Photocatalytic Oxidation of Hazardous Organic Contaminants in Water." *Water Environment Research* 65 (5): 665–73.

Tang, W. Z., H. An, and An. Huren. 1995. "UV/TiO2 Photocatalytic Oxidation of Commercial Dyes in Aqueous Solutions." *Chemosphere* 31 (9): 4157–70.

Tanwar, S., N. Singh, and A. L. Sharma. 2023. "Fabrication of Activated Carbon Coated MSe2 (M=Mo, Co, and Ni) Nanocomposite Electrode for High-Performance Aqueous Asymmetric Supercapacitor." *Colloids and Surfaces A: Physicochemical and Engineering Aspects* 666: 131235.

Vela, N., M. Calín, M. J. Yáñez-Gascón, I. Garrido, G. Pérez-Lucas, J. Fenoll, and S. Navarro. 2018. "Photocatalytic Oxidation of Six Pesticides Listed as Endocrine Disruptor Chemicals from Wastewater Using Two Different TiO2 Samples at Pilot Plant Scale under Sunlight Irradiation." *Journal of Photochemistry and Photobiology A: Chemistry* 353: 271–8.

Velegraki, T., E. Hapeshi, D. Fatta-Kassinos, and I. Poulios. 2015. "Solar-induced Heterogeneous Photocatalytic Degradation of Methyl-Paraben." *Applied Catalysis B: Environmental* 178: 2–11.

Volkov, D., O. Rogova, and M. Proskurnin. 2021. "Organic Matter and Mineral Composition of Silicate Soils: FTIR Comparison Study by Photoacoustic, Diffuse Reflectance, and Attenuated Total Reflection Modalities." *Agronomy* 11 (9): 1879.

Wang, R., X. Ma, T. Liu, Y. Li, L. Song, S. C. Tjong, L. Cao, W. Wang, Q. Yu, and Z. Wang. 2020. "Degradation Aspects of Endocrine Disrupting Chemicals: A Review on Photocatalytic Processes and Photocatalysts." *Applied Catalysis A: General* 597: 117547.

Wang, Guohong, Lin Xu, Jun Zhang, Tingting Yin, and Deyan Han. 2012. "Enhanced Photocatalytic Activity of TiO_2 Powders (P25) via Calcination Treatment." *International Journal of Photoenergy* 2012, https://doi.org/10.1155/2012/265760.

Wen, Y., F. Wei, W. Zhang, A. Cui, J. Cui, C. Jing, Z. Hu, Q. He, J. Fu, S. Liu, and J. Cheng. 2020. "Two-dimensional Mesoporous Sensing Materials." *Chinese Chemical Letters* 31 (2): 521–4.

WHO. 2003. *Atrazine in Drinking-Water: Background Document for Development of WHO Guidelines for Drinking-Water Quality*. World Health Organization.

Wu, S., H. Li, X. Li, H. He, and C. Yang. 2018. "Performances and Mechanisms of Efficient Degradation of Atrazine Using Peroxymonosulfate and Ferrate as Oxidants." *Chemical Engineering Journal* 353: 533–41.

Yang, J., Q. Wu, S. He, J. Yan, J. Shi, J. Chen, M. Wu, and X. Yang. 2015. "Completely <001> Oriented Anatase TiO 2 Nanoarrays: Topotactic Growth and Orientation-Related Efficient Photocatalysis." *Nanoscale* 7 (33): 13888–97.

Zhang, Y., and K. Pagilla. 2010. "Treatment of Malathion Pesticide Wastewater with Nanofiltration and Photo-Fenton Oxidation." *Desalination* 263 (1–3): 36–44.

Supplementary Material: This article contains supplementary material (https://doi.org/10.1515/ijcre-2022-0186).